Journal of Power Sources 297 (2015) 534–539

Contents lists available at ScienceDirect

Journal of Power Sources

journal homepage: www.elsevier.com/locate/jpowsour

Copper Iron Conversion Coating for Solid Oxide Fuel Cell Interconnects

Jan Gustav Grolig*, Patrik Alnegren, Jan Froitzheim, Jan-Erik Svensson

Environmental Inorganic Chemistry, Chalmers University of Technology, Kemivägen 10, SE-41296 Gothenburg, Sweden

HIGHLIGHTS

- We exposed copper iron coated Sanergy HT in a SOFC cathode side atmosphere.
- Corrosion, chromium evaporation and ASR evolution were monitored.
- Copper iron coated Sanergy HT showed lower corrosion and Chromium evaporation.
- An ASR value of only of 10 mΩcm^2 was reached after 1000 h of exposure.

ARTICLE INFO

Article history:
Received 25 April 2015
Received in revised form
7 June 2015
Accepted 26 June 2015
Available online 25 August 2015

Keywords:
Interconnect
Corrosion
Chromium volatilization
Sanergy HT
SOFC
Area specific resistance

ABSTRACT

A conversion coating of iron and copper was investigated with the purpose of increasing the performance of Sanergy HT as a potential SOFC interconnect material. Samples were exposed to a simulated cathode atmosphere (air, 3 % H_2O) for durations of up to 1000 h at 850 °C. Their performance in terms of corrosion, chromium evaporation and electrical resistance (ASR) was monitored and compared to uncoated and cobalt-coated Sanergy HT samples. The copper iron coating had no negative effects on corrosion protection and decreased chromium evaporation by about 80%. An Area Specific Resistance (ASR) of 10 mΩcm^2 was reached after 1000 h of exposure. Scanning Electron Microscopy revealed well adherent oxide layers comprised of an inner chromia layer and an outer spinel oxide layer.

1. Introduction

Since solid oxide fuel cell technology has been substantially improved and the operational temperature for SOFCs has been lowered in recent years, the use of metallic interconnects has become feasible. Interconnects are elements which connect two (often planar) fuel cell elements with each other. The requirements on interconnects are, besides reasonable costs, a sufficient lifetime and a low degradation rate. Some reports mention interconnects as a major source of price when it comes to total stack costs [1]. The optimization of suitable alloys for interconnect applications has led to the development of steels such as Crofer 22 H, Crofer 22 APU, Sanergy HT or ZMG 232 [2–4]. Steels not specially developed for an SOFC application, such as AISI 441 or AISI 430, have also been mentioned as candidate materials for interconnect applications [5–7]. Regardless of the steel used, metallic interconnects suffer from three major degradation problems; corrosion, chromium evaporation and an increasing electrical resistance. Earlier studies have shown that sufficient performance cannot be reached without the use of protective coatings, which decrease the evaporation of chromium and in some case even decrease oxygen inward diffusion [5,8]. Most suggested coatings for metallic interconnect materials are based on cobalt [9–18]. Cobalt is either used in the form of cobalt manganese spinel coatings or in the form of cobalt conversion coatings. These reports focus on different aspects of these coatings such as the route of preparation, the optimum ratio between cobalt and manganese or the effect of different dopants. The mentioned coating systems add costs to the already expensive alloys, because they either use expensive raw materials and/or expensive production methods. Costs can be reduced in several ways, either one uses thinner coatings, uses pre-coated materials to simplify the interconnect production or one tries to use cheaper materials [19–21]. Additionally, environmental and health aspects must be taken into account when it comes to the use of cobalt [22].

* Corresponding author.
E-mail address: Jan.grolig@chalmers.se (J.G. Grolig).

http://dx.doi.org/10.1016/j.jpowsour.2015.06.139

Alternatives to cobalt spinel coatings are only rarely reported in the literature and are mainly based on either perovskite coatings, such as LSM, LSC or LSCF, or other spinel-type coatings. Lanthanum based perovskite coatings are effective when they are well adherent to the interconnect material, and, since they cannot prevent chromium outward diffusion, they are applied rather thickly [23–26], furthermore material costs are even higher than for cobalt. Perovskite coatings of LSM have been investigated for example by Choi et al. who found good performance for these coating in terms of adhesion and electrical properties; however, they also used very thick (>10 μm) coatings [23]. In contrast Yang et al. used LSCF and LSC which suffered from adhesion problems, and they suspected that chromium evaporation could not be prevented by these types of coatings [24].

Alternative cobalt-free spinel systems have not been as widely reported as cobalt spinels. Some research on copper spinels has been reported by Paulson et al. and Joshi et al. [27–29]. They have found that copper spinels can, when doped with magnesium, improve oxide conductivity and prevent the outward diffusion of chromium. So far no measurements on the evaporation of chromium on copper spinel coated interconnect material have been reported. Zhang et al. have reported on copper iron spinel and nickel manganese spinel coatings, which were considered to be promising for improving, interconnect performance in terms of oxidation [30,31].

Besides perovskite coatings and spinel-type coatings, there have been some reports on other coatings. Nielsen et al. tested nickel-plated ferritic stainless steel in a stack test and found that nickel diffused into the interconnect during the first heating, and they observed austenite formation and a lower chromium outward diffusion than the uncoated material [32]. Johnson et al. tested coatings of $LaCrO_3$ on Crofer 22 APU and SS 446, which showed good performance, but these coatings were sensitive to substrate impurities such as aluminum and silicon [33]. MCrAlYO coatings (in which M can be Ti, Co or Mn) have been reported as another class of coatings by Gannon et al. and Piccardo et al. [34,35]. These advanced phases have showed promise since they exhibit good thermal stability and decreased chromium evaporation, but they can be assumed to be costly when applied in large scale.

Petric and Ling did a comprehensive study on the suitability of binary spinel systems for an interconnect coating application in terms of the coefficient of thermal expansion and electrical properties [36]. They concluded that in addition to the well-reported cobalt manganese spinels, spinels of copper and manganese and copper and iron are the most promising candidate materials for interconnect coatings.

The present research is, therefore, based on a copper iron conversion coating, which is assumed to form a copper iron spinel during oxidation. The reason for this is because the first findings on these kinds of coatings appear to be promising in terms of corrosion and chromium evaporation properties [20]. Additionally, considering factors such as material costs and availability, it is worthwhile to investigate such a material as a potential interconnect coating. For this reason, corrosion, chromium evaporation and electrical properties were investigated and combined with XRD and electron microscopy.

2. Experimental

2.1. Sample preparation

Uncoated and pre-coated steel sheets of Sanergy HT, with a thickness of 0.2 mm, were received from Sandvik Materials Technology. The composition of the substrate material is given in Table 1. The coated samples were covered with a three-layer coating using an industrially available physical vapor deposition method and consisted of a first layer of iron 50 nm thick, then a 400 nm layer of copper and an 800 nm layer of iron. The first iron coating layer was applied to achieve better adhesion. The cobalt coated samples, which were already intensively studied in earlier studies had a film thickness of approximately 600 nm [37,38]. The sheets were thereafter cut into coupons of 15 × 15 mm^2. After ultrasonic cleaning with acetone and ethanol, the samples were weighed using an XT6 scale (Mettler Toledo).

2.2. Exposure

The samples were exposed at 850 °C in tubular furnaces in simulated cathode atmosphere (air, 3 % water vapor, average gas flow velocity of 27 cm/s) more information can be found in [16]. The water content was adjusted with a coil condenser and was maintained at thermodynamic equilibrium [16]. The samples were exposed isothermally. The evaporation of chromium was measured using the Denuder Technique [16]. The outlet of the furnace was equipped with a so-called denuder tube, which was coated with sodium carbonate. The sodium carbonate is reacting with gaseous chromium species and, by exchanging the denuder tube in regular intervals, chromium evaporation can be measured in a time resolved manner. The denuder tubes have been washed with MQ water and the wash solutions have been analyzed for chromium content by photo-spectrometry. The accuracy of the measurement technique has been previously determined to be 95 ± 5 %.

2.3. Analysis

A Siemens D 5000 grazing incidence diffractometer was used to characterize the crystal structure of the oxide layers. The angle of incidence was set to 2° and CuKα radiation was used. Mechanical cross-sections for SEM and EDX analyses (LEO Ultra 55 FEG SEM) were prepared using epoxy embedding and classical polishing methods. Before embedding, a protective nickel coating was applied to the samples via electro-plating.

2.4. Area-specific resistance measurement

The samples were prepared for ASR characterization as reported in a previous study [39]: A pre-oxidized sample was masked with a shadow mask of 10 × 10 mm^2 and sputtered with platinum using a Quorum 150 sputter coater (60 mA and 10 min duration) to ensure a defined electrode area, which is approximately 100 nm thick. This procedure was repeated for the other side of the sample. The electrodes were repainted with platinum ink (Metalor 6082) using a fine brush to obtain an electrode thickness of about several μm. The samples were then dried for 1.5 h at 150 °C and fired at 850 °C for 10 min to burn off the binder of the platinum ink. The prepared samples were placed into a Probostat® (Norecs) sample holder with a four-point setup which was placed into a tubular furnace. The duration of measurement was kept at an absolute minimum to avoid platinum influencing the oxide scale morphology as reported previously [39]. The DC resistance was measured on two different test stands using either a Keithley 2440 Current Source in combination with a Keithley 2701 digital multimeter or using only a Keithley 2400 in four-point mode. A current density of 100 mA/cm^2 was applied during the measurement, and the ASR was measured in 50 °C increments from 850 °C down to 500 °C to enable an activation energy calculation.

Table 1
Sanergy HT composition in wt. % given by the supplier.

Fe	C	Si	Mn	P	S	Cr	Ni	Mo	W	Cu	Nb	Ti	N	Zr
Bal.	0.01	0.07	0.25	0.013	0.0005	22.39	0.81	0.93	<0.01	0.017	0.41	0.06	0.024	0.06

3. Results

3.1. Mass gain and chromium evaporation

The copper-iron-coated samples' mass gain has been plotted in Fig. 1 and is represented by filled circles. The mass gain of uncoated Sanergy HT, represented by hollow squares, and cobalt-coated Sanergy HT, represented by triangles, were added for comparison. The initial mass gain of approximately 0.37 mg/cm^2 is due to the oxidation of the copper and iron coating. This initial mass gain appeared to be an effect similar to the observed initial mass gain of cobalt-coated Sanergy HT of 0.21 mg/cm^2 reported earlier [5,19,37–39]. The mass gain of the copper-iron-coated samples seems to follow a trend similar to the uncoated substrate material – only shifted for the initial mass gain (see dashed line for comparison). Additionally the cobalt-coated samples exhibited a slightly higher mass gain at longer exposure times than the copper iron coated samples. After an exposure time of 1000 h, a mass gain of about 1.0 mg/cm^2 was reached for the copper iron coated samples, compared to 0.6 mg/cm^2 and 1.17 mg/cm^2 for the uncoated and the cobalt-coated Sanergy HT samples, respectively.

The cumulated evaporation of chromium is shown in Fig. 2. Uncoated Sanergy HT and cobalt-coated Sanergy HT have been added for comparison. The copper iron coated samples showed about an 80 % reduction of chromium evaporation compared to the uncoated substrate material, which can be compared to a 90 % reduction of chromium evaporation found for the cobalt coating. Overall chromium evaporation followed an almost linear trend in the investigated time frame. A value of 6.7*10^{-4} kg/m^2 of evaporated chromium was reached for copper iron coated samples after 1000 h of exposure, and 3.2*10^{-4} kg/m^2 was reached for the cobalt-coated samples after approximately the same time, whereas the uncoated samples had evaporated 24.1*10^{-4} kg/m^2 of chromium after only 750 h of exposure. The rate of chromium evaporation was 5.7*10^{-7} kg/m^2/h for the copper iron coated samples, 3.08*10^{-7} kg/m^2/h for the cobalt coated samples and 3.3*10^{-6} kg/m^2/h for the uncoated samples after about 500 h of exposure.

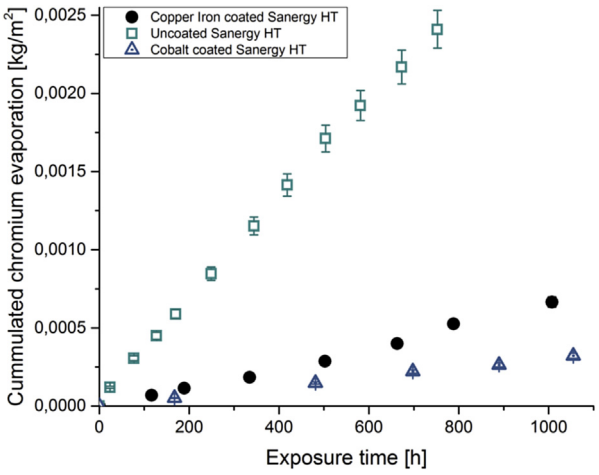

Fig. 2. Chromium evaporation of copper iron coated Sanergy HT exposed at 850 °C in air, cobalt and uncoated Sanergy HT for comparison.

3.2. Electrical properties

The evolution of the Area Specific Resistance (ASR) can be seen in Fig. 3. The ASR values of cobalt-coated samples have been added for comparison. Due to interaction of uncoated Sanergy HT with the platinum electrode, similar to the observations of an earlier study, the values were not considered as reliable and were, therefore, excluded from the plot [39]. Since several samples were measured for each time period and due to the nature of ASR measurements, a significant spread was observed, which is represented in the error bars. After 1000 h of exposure, an ASR value of about 10 mΩcm^2 was obtained for one oxide scale of the copper iron coated samples and in comparison 13 mΩcm^2 for the cobalt-coated samples. The activation energy for the electronic conduction, derived from the measurements at various temperatures during the cooling of the setup, was relatively similar for all measured copper iron coated

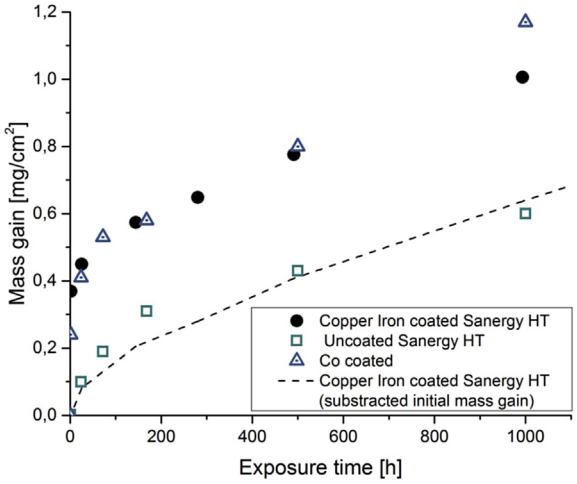

Fig. 1. Mass gain of copper iron coated Sanergy HT exposed at 850 °C in air, cobalt and uncoated Sanergy HT for comparison.

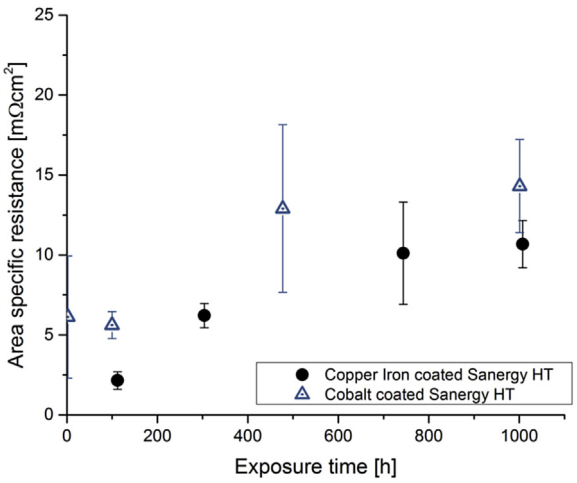

Fig. 3. Area specific resistance of copper iron coated Sanergy HT exposed at 850 °C in air, cobalt coated Sanergy HT for comparison.

samples. The activation energy estimated for the electronic conduction varied for all samples between 0.64 eV and 0.54 eV and a trend towards lower activation energy was observed, however, the observed trend lied within the error margins.

3.3. Microstructural evolution

An XRD diffraction pattern for a copper iron coated sample exposed for 1000 h is depicted in Fig. 4. Two phases could be identified with the use of the database; an eskolaite phase (space group 167, R-3c) and a spinel phase (space group 227, Fd-3m). Peaks are indicated in the figure by symbols below the scan; stars for eskolaite (chromium oxide) and triangles for spinel (copper manganese iron oxide). Additionally, two cross-sectional SEM micrographs are shown in Fig. 5 (after 100 h of exposure) and Fig. 7 (after 1000 h of exposure). Both reveal a layered oxide scale structure, which is well adhered to the substrate material. The oxide morphology was divided into three regions (see Figs. 5 and 7); Region 1 – the outer oxide scale, Region 2 – the inner oxide scale and Region 3 the substrate.

Two EDX maps were recorded for a sample exposed for 100 h (Fig. 6) and a sample exposed for 1000 h (Fig. 8). The outer oxide (Region 1) was mainly composed of iron, manganese and copper oxide. Also a small quantity of chromium was detected in the outer oxide scale, however, it cannot be excluded that this chromium signal stems from the underlying Cr_2O_3 layer. Some pores were seen in the outer oxide scale and might be due to sample preparation, since the samples were mechanically polished before SEM investigation. The inner oxide (Region 2) of these samples was mainly composed of chromium oxide with a small amount of manganese, and the substrate had a composition comparable to the "as received" substrate. It can be seen in the figures that the inner chromium oxide layer grew significantly in thickness from 1–2 μm to 4–5 μm, whereas the outer oxide thickness remained relatively constant in both cases with 2–3 μm thickness. It can clearly be seen that in the outer oxide after only 100 h of exposure a copper and manganese rich layer is separated from an iron rich layer at the surface. This layered structure within the outer oxide is not observed after 1000 h of exposure, as it seems that the cation distribution has evened out. The chemical composition of the inner oxide layer seemed to stay constant over the investigated time frame and seemed to be just increased in thickness, in contrast to the outer oxide layer.

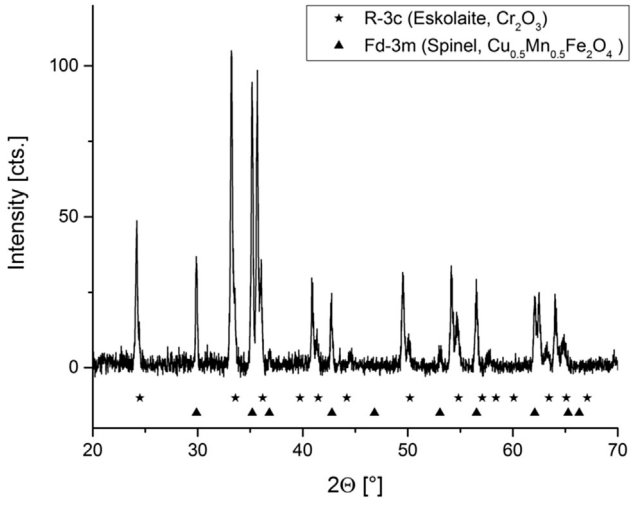

Fig. 4. XRD grazing incidence scan of copper iron coated sample after 1000 h of exposure at 850 °C in air.

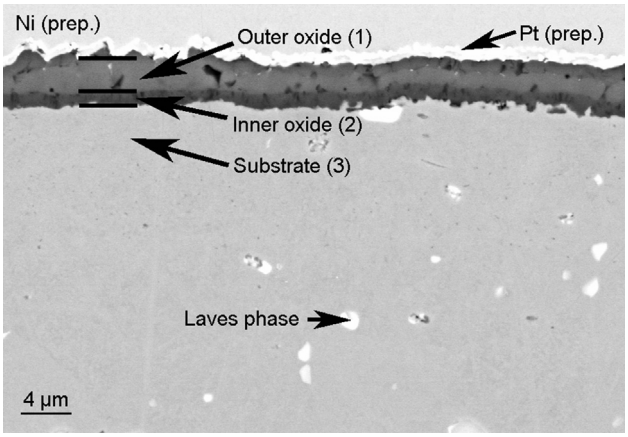

Fig. 5. Cross-section of a copper iron coated Sanergy HT sample exposed for 100 h at 850 °C in air.

4. Discussion

4.1. Corrosion properties and chromium evaporation

The copper iron coated Sanergy HT samples showed a mass gain curve similar to the uncoated material after subtracting the initial mass gain from the oxidation of the metallic coating of about 0.37 mg/cm^2. It seems that the coating did not accelerate nor decrease the rate of oxidation. That is not taking into account that the coated material evaporates about 80 % less chromium. This corresponds to a weight loss of approximately 0.3 mg/cm^2 for the uncoated material compared to 0.07 mg/cm^2 for the copper iron coated material. This means that the uncoated material oxidizes faster. This observation is similar to findings for cobalt coatings investigated earlier [37,38]. But due to the relatively high exposure temperature and the relatively low thickness, the copper iron spinel is expected to have a too high oxygen diffusion coefficient, thus does not slow down the oxygen inward diffusion. This in itself might result in an oxygen supply to the chromia scale which is too high to be rate limiting for the oxidation and thus the improvement in corrosion protection is probably only due to less chromium depletion. Both the copper iron coating and the inner chromium oxide layer were well adherent to the substrate material throughout the entire investigated time frame, which is an essential property for a potential long-term operation [40]. The two phases identified in the XRD analysis can be linked to an outer spinel layer and an inner eskolaite layer, based on the composition found with EDX analysis. Since the copper iron coated samples showed a decrease in the evaporation of chromium, better long-term stability and better corrosion protection should be expected from this coating when exposed for longer times, due to lower chromium depletion of the substrate. The amount of evaporated chromium was about twice as much for the copper iron coated samples as for cobalt coated Sanergy HT. This might be due to the higher chromium activity on the oxide surface as was seen in the EDX analysis, due to a potentially higher chromium diffusion coefficient in the copper iron spinel compared to a cobalt manganese spinel. Additionally, significant amounts of manganese were also present in the outer oxide scale of the copper iron coated samples after 1000 h of exposure. The phenomenon of manganese outward diffusion has been observed in previous investigations on cobalt coatings [5,37–39]. From an application point of view, this could be detrimental for the copper iron coating in two ways; manganese

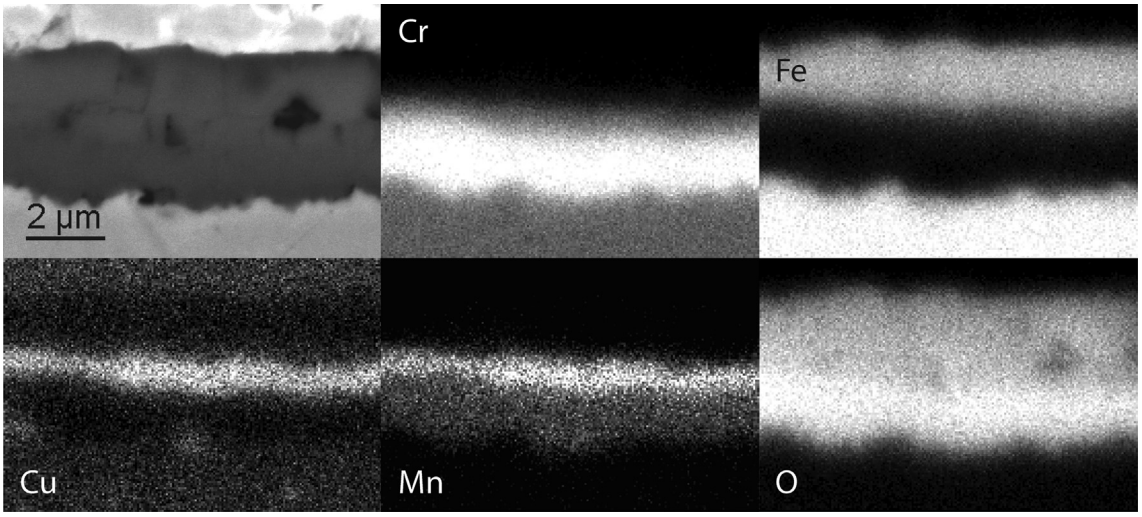

Fig. 6. EDX map of a copper iron coated Sanergy HT sample exposed for 100 h at 850 °C in air.

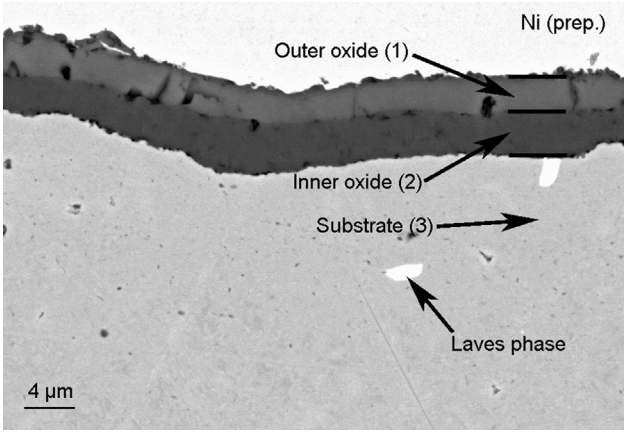

Fig. 7. Cross-section of a copper iron coated Sanergy HT sample exposed for 1000 h at 850 °C in air.

increases the lattice parameter of the iron copper spinel, as seen in Salah et al. [41], which might increase chromium outward diffusion, if the dominant diffusion mechanism is by lattice diffusion. Secondly, higher content of manganese decreases the electrical conductivity [41]. This effect can be expected to be less pronounced when thicker coatings are used since the manganese would be more diluted.

4.2. ASR performance

The increasing ASR of the interconnects used in a solid oxide fuel cell stack is one of the main sources of performance loss and a target of 100 mΩcm^2 has been defined for long-term operation (>40.000 h). This translates into 50 mΩcm^2 for one oxide scale [42]. The investigated copper iron coated Sanergy HT had an ASR value of about 10 mΩcm^2 after 1000 h of exposure at 850 °C. The evolution of ASR values followed a trend similar to the mass gain of the samples, if the initial mass gain is neglected. Therefore, it might be assumed that the major part of the ASR values is mainly dependent on the growing inner chromia oxide scale, since the outer oxide scale remained relatively constant in thickness (Figs. 5 and 6) and is expected to be far more conductive than chromia. Additionally, a very low ASR value of about 2 mΩcm^2 was measured after 100 h of exposure, and Fig. 5 reveals a very thin chromia layer for this exposure time. Consequently, it might be assumed that the ASR of only the outer oxide scale is well below 2 mΩcm^2. This would support the assertion that the ASR is mainly dependent on chromia thickness for longer exposure times.

There are no literature values available for copper iron coatings on ferritic steels. Based on the literature review of Ling and Petric for various duplex spinel compounds, better conductivity for cobalt-coated Sanergy HT than for the copper iron coated samples would be expected. This is not in line with the observation made in this study, since the ASR values of the cobalt-coated samples were slightly higher than the ASR values of the copper iron coated samples. The copper iron spinel formed in this study was far from pure and contained substantial amounts of manganese and chromium, and, for this reason, a comparison to literature values is less reasonable. However, because impurities can add energy levels within the band gap, better conductivities might be suspected for the outer spinel layer in the copper iron coated sample. The same holds true for the inner chromia layer, which contained some amounts of manganese, which might improve the conductivity of chromia as well.

Since the operation temperature of solid oxide fuel cell stacks is usually not as high as the selected experimental temperature in this study, a significant reduction of the thickness of the chromia layer might be expected. Thus, an even better ASR performance for copper iron coated interconnects would be expected when these are used at low temperatures. However, a lower inter-diffusion of manganese, iron and chromium might decrease the expected ASR improvement slightly, since the oxide scales might become more pure when this type of substrate coating combination is used at lower temperatures.

5. Conclusion

A coating of 400 nm copper and 800 nm iron was investigated as a conversion coating for ferritic stainless steel interconnect material. After exposure, a manganese copper iron spinel oxide layer was observed on the surface of the sample. The spinel layer covered a chromium oxide layer, and both oxides were well-adhered to the sample surface. The mass gain of the coated samples followed, after

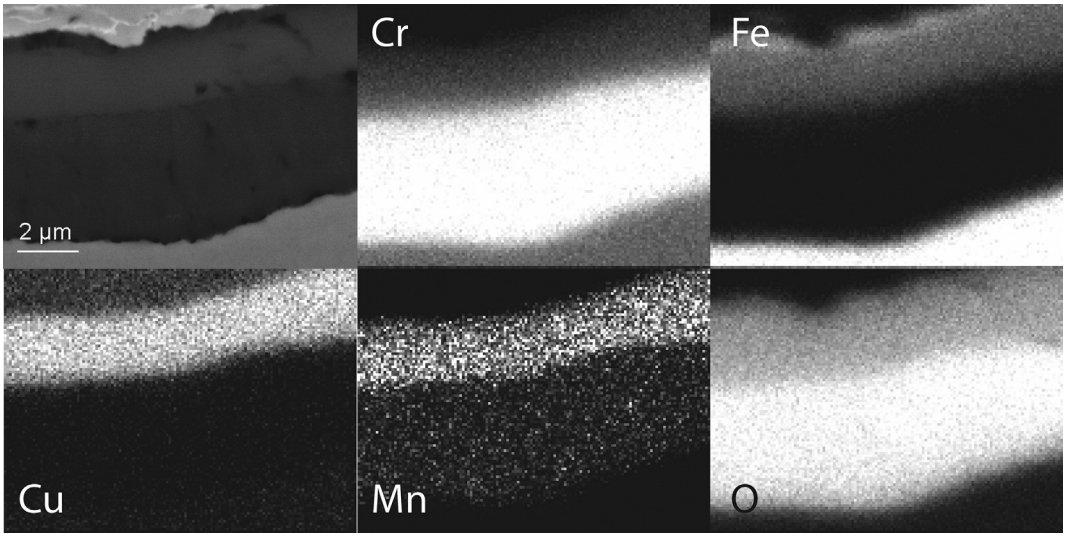

Fig. 8. EDX map of a copper iron coated Sanergy HT sample exposed for 1000 h at 850 °C in air.

subtracting the initial mass gain, a trend similar to the uncoated substrate material. The evaporation of chromium could be reduced by about 80 % compared to the uncoated substrate material. The evolution of ASR values reached a value of 10 mΩcm^2 after 1000 h of exposure. It can be concluded that this coating is promising for further investigations. Future studies of these kinds of coatings should examine different pre-oxidation procedures, thicker coatings and lower exposure temperatures.

Acknowledgments

The authors gratefully acknowledge the financial support from the METSAPP project, grant number 278257, The Swedish Research Council and the Swedish Energy Agency (Grant Agreement No 34140-1), and the Swedish High Temperature Corrosion Center (HTC). Rakshith Nugehalli Sachitanand is gratefully acknowledged for his valuable input during the discussions and for proof reading this paper.

References

[1] T.D. Hall, H.A. McCrabb, J. Wu, H. Zhang, X. Liu, E.J. Taylor, Electrodeposition of CoMn onto stainless steels interconnects for increased lifetimes in SOFCs, in: S.C. Singhal, K. Eguchi (Eds.), Solid Oxide Fuel Cells 12, Electrochemical Society Inc, Pennington, 2011, pp. 2489–2502.
[2] R. Sachitanand, M. Sattari, J.E. Svensson, J. Froitzheim, Int. J. Hydrogen Energy 38 (2013) 15328–15334.
[3] D.E. Alman, P.D. Jablonski, Int. J. Hydrogen Energy 32 (2007) 3743–3753.
[4] M. Stanislowski, E. Wessel, K. Hilpert, T. Markus, L. Singheiser, J. Electrochem. Soc. 154 (2007) A295–A306.
[5] J.G. Grolig, J. Froitzheim, J.E. Svensson, J. Power Sources 248 (2014) 1007–1013.
[6] P.D. Jablonski, C.J. Cowen, J.S. Sears, J. Power Sources 195 (2010) 813–820.
[7] I. Belogolovsky, P.Y. Hou, C.P. Jacobson, S.J. Visco, J. Power Sources 182 (2008) 259–264.
[8] P. Wei, X. Deng, M.R. Bateni, A. Petric, Corrosion 63 (2007) 529–536.
[9] W. Qu, L. Jian, D.G. Ivey, J.M. Hill, J. Power Sources 157 (2006) 335–350.
[10] C.J.D. Kumar, A. Dekich, H. Wang, Y. Liu, W. Tilson, J. Ganley, J.W. Fergus, J. Electrochem. Soc. 161 (2014) F47–F53.
[11] Z. Yang, G. Xia, S.P. Simner, J.W. Stevenson, J. Electrochem. Soc. 152 (2005) A1896–A1901.
[12] J.W. Wu, C.D. Johnson, Y.L. Jiang, R.S. Gemmen, X.B. Liu, Electrochim. Acta 54 (2008) 793–800.
[13] S. Molin, B. Kusz, M. Gazda, P. Jasinski, J. Solid State Electrochem. 13 (2009) 1695–1700.
[14] J. Puranen, M. Pihlatie, J. Lagerbom, G. Boleili, J. Laakso, L. Hyvarinen, M. Kylmalahti, O. Himanen, J. Kiviaho, L. Lusvarghi, P. Vuoristo, Int. J. Hydrogen Energy 39 (2014) 17284–17294.
[15] A. Kruk, M. Stygar, T. Brylewski, J. Solid State Electrochem. 17 (2013) 993–1003.
[16] J. Froitzheim, H. Ravash, E. Larsson, L.G. Johansson, J.E. Svensson, J. Electrochem. Soc. 157 (2010) B1295–B1300.
[17] Q.X. Fu, D. Sebold, F. Tietz, H.P. Buchkremer, Solid State Ion. 192 (2011) 376–382.
[18] X.H. Deng, P. Wei, M.R. Bateni, A. Petric, J. Power Sources 160 (2006) 1225–1229.
[19] J. Froitzheim, J.E. Svensson, Multifunctional nano-coatings for SOFC interconnects, in: S.C. Singhal, K. Eguchi (Eds.), Solid Oxide Fuel Cells 12, Electrochemical Society Inc, Pennington, 2011, pp. 2503–2508.
[20] J.G. Grolig, H. Abdesselam, M. Gas, H.F. Windisch, J. Froitzheim, J.E. Svensson, Solid Oxide Fuel Cells 13 (Sofc Xiii) 57 (2013) 2339–2347.
[21] J. Froitzheim, A. Magraso, T. Holt, M.W. Lundberg, H.F. Windisch, R. Berger, R. Sachitanand, J. Westlinder, J.E. Svensson, R. Haugsrud, Solid Oxide Fuel Cells 13 (Sofc Xiii) 57 (2013) 2187–2193.
[22] D.G. Barceloux, J. Toxic. Clin. Toxicol. 37 (1999) 201–216.
[23] J.J. Choi, D.S. Park, B.D. Hahn, J. Ryu, W.H. Yoon, J. Am. Ceram. Soc. 91 (2008) 2601–2606.
[24] Z.G. Yang, G.G. Xia, G.D. Maupin, J.W. Stevenson, J. Electrochem. Soc. 153 (2006) A1852–A1858.
[25] M. Stanislowski, J. Froitzheim, L. Niewolak, W.J. Quadakkers, K. Hilpert, T. Markus, L. Singheiser, J. Power Sources 164 (2007) 578–589.
[26] H. Kurokawa, C.P. Jacobson, L.C. DeJonghe, S.J. Visco, Solid State Ion. 178 (2007) 287–296.
[27] S.C. Paulson, M.R. Bateni, P. Wei, A. Petric, V.I. Birss, Improving LSM cathode performance using $(Cu,Mn)_3O_4$ spinel coated UNS430 ferritic stainless steel SOFC interconnects, in: K. Eguchi, S.C. Singhai, H. Yokokawa, H. Mizusaki (Eds.), Solid Oxide Fuel Cells 10, Electrochemical Society Inc, Pennington, 2007, pp. 1097–1106.
[28] S. Joshi, C. Silva, A. Petric, Solid State Ion. Devices 9 Ion. Conduct. Thin Films Multilayers 50 (2013) 153–160.
[29] S. Joshi, C. Silva, P. Wang, Y. Mozharivskyj, A. Petric, J. Electrochem. Soc. 161 (2014) F233–F238.
[30] W.Y. Zhang, B. Hua, N.Q. Duan, J. Pu, B. Chi, J. Li, J. Electrochem. Soc. 159 (2012) C388–C392.
[31] W.Y. Zhang, J. Pu, B. Chi, L. Jian, J. Power Sources 196 (2011) 5591–5594.
[32] K.A. Nielsen, A.R. Dinesen, L. Korcakova, L. Mikkelsen, P.V. Hendriksen, F.W. Poulsen, Fuel Cells 6 (2006) 100–106.
[33] C. Johnson, N. Orlovskaya, A. Coratolo, C. Cross, J. Wu, R. Gemmen, X. Liu, Int. J. Hydrogen Energy 34 (2009) 2408–2415.
[34] P. Gannon, M. Deibert, P. White, R. Smith, H. Chen, W. Priyantha, J. Lucas, V. Gorokhousky, Int. J. Hydrogen Energy 33 (2008) 3991–4000.
[35] P. Piccardo, R. Amendola, S. Fontana, S. Chevalier, G. Caboches, P. Gannon, J. Appl. Electrochem. 39 (2009) 545–551.
[36] A. Petric, H. Ling, J. Am. Ceram. Soc. 90 (2007) 1515–1520.
[37] J. Froitzheim, S. Canovic, M. Nikumaa, R. Sachitanand, L.G. Johansson, J.E. Svensson, J. Power Sources 220 (2012) 217–227.
[38] S. Canovic, J. Froitzheim, R. Sachitanand, M. Nikumaa, M. Halvarsson, L.G. Johansson, J.E. Svensson, Surf. Coat. Technol. 215 (2013) 62–74.
[39] J.G. Grolig, J. Froitzheim, J.-E. Svensson, J. Power Sources 284 (2015) 321–327.
[40] W.J. Quadakkers, J. Piron-Abellan, V. Shemet, L. Singheiser, Mater. High. Temp. 20 (2003) 115–127.
[41] L.M. Salah, A.M. Moustafa, I.S.A. Farag, Ceram. Int. 38 (2012) 5605–5611.
[42] W.Z. Zhu, S.C. Deevi, Mater. Res. Bull. 38 (2003) 957–972.